Analysis of the Ion Energy Transport in Ohmic Discharges in the ASDEX Tokamak

E.E. Simmet, H.-U. Fahrbach, W. Herrmann, U. Stroth

IPP III/215

October 1996

MAX-PLANCK-INSTITUT FÜR PLASMAPHYSIK

85748 GARCHING BEI MÜNCHEN

MAX-PLANCK-INSTITUT FÜR PLASMAPHYSIK

GARCHING BEI MÜNCHEN

Analysis of the Ion Energy Transport in Ohmic Discharges in the ASDEX Tokamak

E.E. Simmet, H.-U. Fahrbach, W. Herrmann, U. Stroth

IPP III/215 October 1996

Die nachstehende Arbeit wurde im Rahmen des Vertrages zwischen dem Max-Planck-Institut für Plasmaphysik und der Europäischen Atomgemeinschaft über die Zusammenarbeit auf dem Gebiete der Plasmaphysik durchgeführt.

Analysis of the Ion Energy Transport in Ohmic Discharges in the ASDEX Tokamak

E.E. Simmet, H.–U. Fahrbach, W. Herrmann, U. Stroth

Max–Planck–Institut für Plasmaphysik,
EURATOM–IPP Association,
Garching/München, Germany

Abstract: An analysis of the local ion energy transport is performed for more than one hundred well documented ohmic ASDEX discharges. These are characterized by three different confinement regimes: the linear ohmic confinement (LOC), the saturated ohmic confinement (SOC) and the improved ohmic confinement (IOC). All three are covered by this study.

To identify the most important local transport mechanism of the ion heat, the ion power balance equation is analyzed. Two methods are used: straightforward calculation with experimental data only, and a comparison of measured and calculated profiles of the ion temperature and the ion heat conductivity, respectively. A discussion of the power balance shows that conductive losses dominate the ion energy transport in all ohmic discharges of ASDEX. Only inside the q=1–surface losses due to sawtooth activity play a role, while at the edge convective fluxes and CX–losses influence the ion energy transport. Both methods lead to the result that both the ion temperature and the ion heat conductivity are consistent with predictions of the neoclassical theory. Enhanced heat losses as suggested by theories eg. on the basis of η_i modes can be excluded.

1 Introduction

In ohmic discharges only the electrons are heated by external means. The energy gain of the ions results from energy exchange between the ions and the "hot" electrons. The energetic equilibrium of the ions is a direct consequence of internal transport mechanisms. Especially the heating of the ions and also their losses via heat conduction and diffusion are not influenced externally.

For ohmic discharges three regimes can be distinguished due to the different quality of the energy confinement (s. Fig. 1). For low densities the global confinement time τ_E increases nearly linearly with increasing line–averaged plasma density (LOC regime). If a critical density is reached, τ_E saturates. At ASDEX this density is approximately 3×10^{19} m^{-3}. For higher densities the confinement time stays on a constant level (SOC regime) of about 80–90 ms for deuterium plasmas and 50–60 ms for hydrogen plasmas. For the same density range a further regime with improved confinement (IOC regime) is reached in deuterium plasmas only, if the external flux of neutral gas into the plasma is reduced [1]. Similar to the LOC, the confinement time increases with the density. Values of up to 120–130 ms are possible at the highest densities.

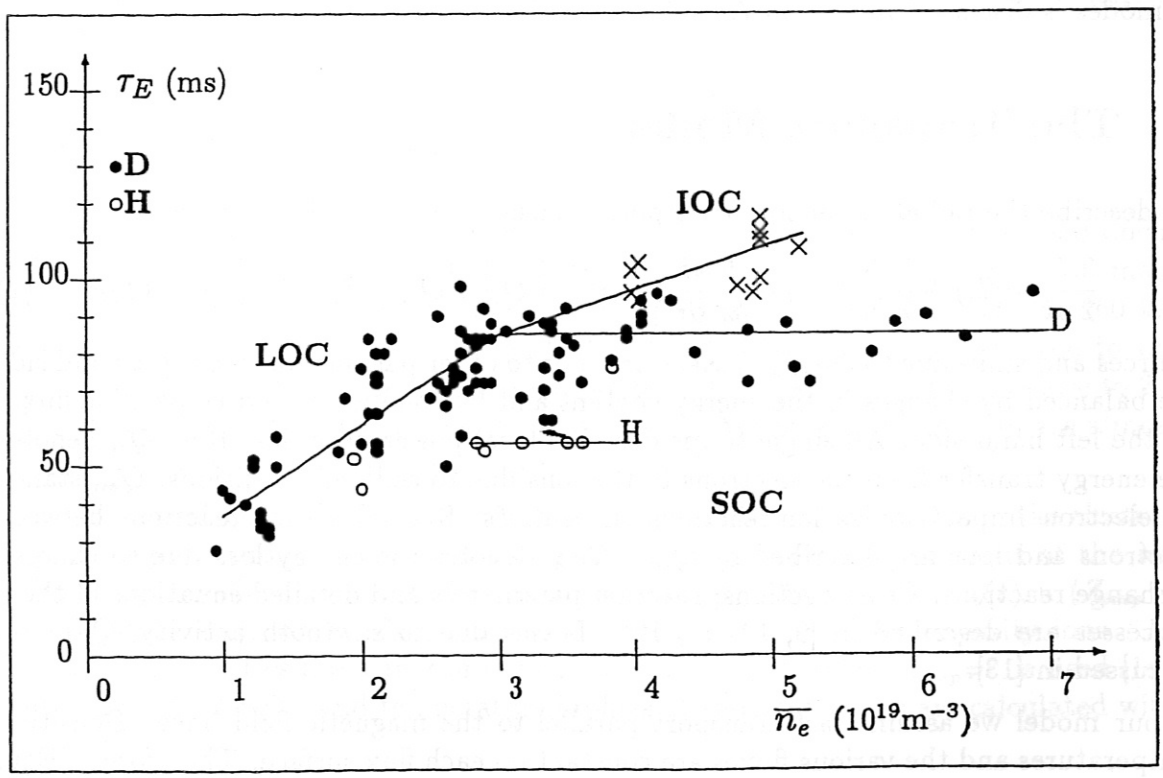

Figure 1: Energy confinement time in ohmic discharges in ASDEX. Due to different dependencies on the line averaged density three confinement regimes are defined: LOC (low density, linear τ_E), SOC (high density, saturation) and IOC (high density, again linear), respectively.

Due to analyses of global data, the behaviour of τ_E in the LOC and SOC regimes was frequently attributed to anomalous ion energy transport mainly caused by η_i modes [2, 3, 4]. These modes are suppressed in IOC discharges. This regime is explained by recovering neoclassical ion losses. For ASDEX, an enhancement factor around 3 above the neoclassical ion transport for LOC and SOC discharges and a neoclassical ion transport for IOC discharges are reported in [5, 6].

As shown in [7] the behaviour of the energy confinement time τ_E in ASDEX is mainly caused by the electron energy transport. Hence, the properties of the ion energy transport cannot be addressed to any mechanism by analysing τ_E only. For this purpose full local analyses of the ion energy balance equation are needed.

Here we present a detailed analysis of the local energy transport in more than 100 ohmic discharges in ASDEX.

The paper is organized in the following way: In section 2 we present the system of equations needed to solve for the ion energy transport. In section 3 experimental data are discussed. These results are used in section 4 to discuss the local power balance equation for the ion energy transport, taking into account all important loss channels. In section 5 we present our results of the ion heat transport in ohmic discharges, especially of the ion heat conductivity. In section 6 our experimental results are compared with the neoclassical predictions as formulated by Chang and Hinton [8]. Finally, the role of η_i modes is discussed in section 7.

2 The Transport Model

To describe the radial ion energy transport we use the power balance equation

$$\frac{3}{2}\frac{\partial}{\partial t}(n_i T_i) + \frac{1}{r}\frac{\partial}{\partial r}(r q_i) + \frac{5}{2r}\frac{\partial}{\partial r}(r T_i \Gamma_i) = Q_{ei} + Q_{eii} - Q_{rec} - Q_{CX} - Q_{ST} \qquad (1)$$

Sources and sinks due to energy transfer from or to other particles on the right hand side are balanced by changes in the energy content and by conductive and convective fluxes on the left hand side. All single terms describe local power densities. Here Q_{ei} denotes the energy transfer from the electrons to the ions due to coulomb–collisions. Q_{eii} stands for electron–impact–ionization reactions on neutrals. Recombination reactions between electrons and ions are described by Q_{rec}. Q_{CX} denotes the energy loss due to charge–exchange reactions. Cross–sections, reaction parameters and detailed equations of these processes are described in [9, 10, 11, 12]. Losses due to sawtooth activity, Q_{ST}, are discussed in [13].

In our model we assume fast transport parallel to the magnetic field lines. Densities, temperatures and the various fluxes are constant on each flux surface. Therefore in Equ. (1) only radial fluxes (perpendicular to the flux surface) and radial derivatives are kept.

For our purpose the integro–differential form

$$\frac{\partial}{\partial t}E_i(r) + P_{hc,i}(r) + P_{conv}(r) = P_{ei}(r) + P_{eii}(r) - P_{rec}(r) - P_{CX}(r) - P_{ST}(r) \qquad (2)$$

gives the better and more accurate results. To get this equation an integration of Equ. (1) over the whole volume inside a flux surface with radius r is performed. The terms on the RHS are now the powers transferred inside this surface and are written in the same order as their related power–densities in Equ. (1). The terms at the LHS are kept in their original order, too. E_i denotes the total ion energy inside the flux–surface. As in this work only data from stationary ohmic discharges are considered, its time–derivative is vanishing. The conductive energy flux of the ions is given by

$$P_{hc,i}(r) = -4\pi^2 R r n_i(r) \chi_i(r) \frac{\partial T_i(r)}{\partial r} \quad , \tag{3}$$

where R is the major radius and χ_i stands for the ion heat conductivity. The convective energy flux is defined as

$$P_{conv}(r) = \frac{5}{2} \times 4\pi^2 R r T_i(r) \Gamma_i(r) \quad . \tag{4}$$

Since the convective energy flux is a product of the ion temperature and the particle flux Γ_i, it is calculated by solving the balance equation for the ion density, including sources and losses due to electron impact ionization reactions and recombination processes.

We make use of the fact that for all ohmic discharges in ASDEX the flux surfaces have approximately circular cross-sections. The Shafranov–shift is included in our numerical algorithm.

3 Experimental Data

For our analyses of the local ion energy transport more than one hundred well documented ohmic discharges are used (LOC: $\approx$ 55, SOC: $\approx$ 45, IOC: $\approx$ 10). The main plasma parameters of the LOC and SOC discharges are: B_t: 1.7–2.8 T, I_p: 220–460 kA and Z_{eff} (in the plasma centre): 1.1–6 (LOC), 1.1–3 (SOC), respectively. Due to the restriction to completely documented radial profiles, IOC discharges with B_t close to 2.8 T, I_p about 360–380 kA and Z_{eff} close to 2 are used. Major and minor radii are almost constant at 165 cm and 40 cm, respectively.

For the local analysis of the ion power balance (Eqs. (1, 2)) radial profiles of the electron and ion densities and temperatures are needed. As a direct measurement of the ion density is not available, n_i is derived from n_e and Z_{eff} by $n_i(r) = n_e(r) \times (Z_{imp} - Z_{eff}(r))/(Z_{imp} - 1)$, where Z_{imp} denotes an average charge of all impurity ions. At ASDEX the impurities are a mix of carbon and oxygen, therefore Z_{imp}=7 is used [14]. Additionally the density and temperature profiles of the neutral gas are calculated with a Monte–Carlo code.

The electron density and temperature are measured by Thomson scattering [15]. The Z_{eff} profile is obtained from a multichord bremsstrahlung measurement [16]. During the stationary phases the electron data were averaged over a few hundred milliseconds. The statistical errors of $n_e(r)$ and $T_e(r)$ are below six per cent. These errors include two types of possible inaccuracies: Due to the averaging, the statistical error of the measured

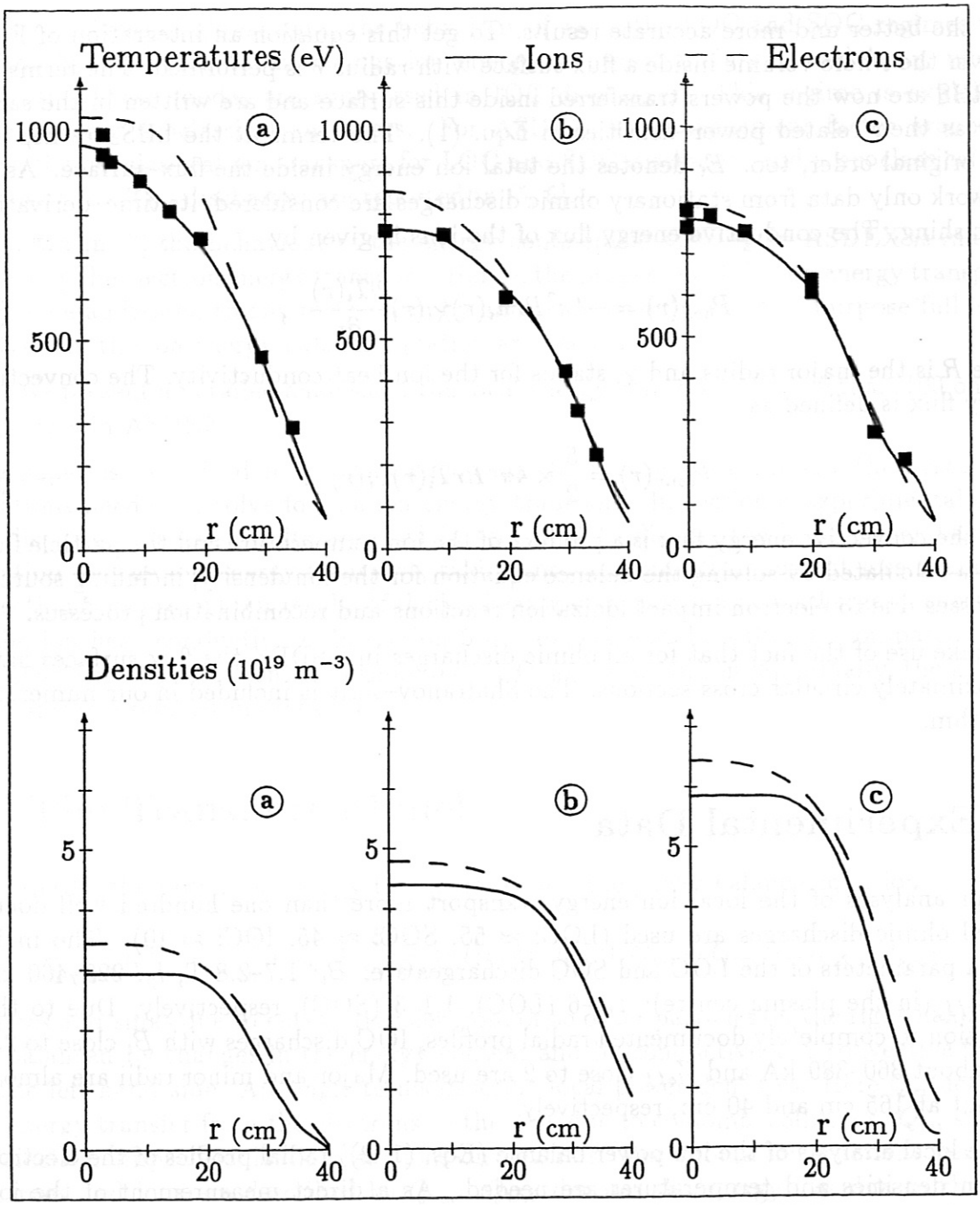

Figure 2: Typical radial profiles of the ion and electron temperatures and densities in ohmic discharges. They belong to plasmas with B_t=2.2 T, I_P=380 kA and line averaged densities of 2.5 (LOC) (a), 4.0 (SOC) (b) and 4.8×10^{19} m^{-3} (IOC) (c).

parameters is in the range of 2 to 4%. An additional error in the range of 2 to 4% arises from the small but non–vanishing shot to shot variance.

Typical profiles for ohmic discharges are shown in Figs. 2. They represent plasmas with B_t=2.2 T, I_P=380 kA and line–averaged electron densities of 2.5 (LOC), 4.0 (SOC) and

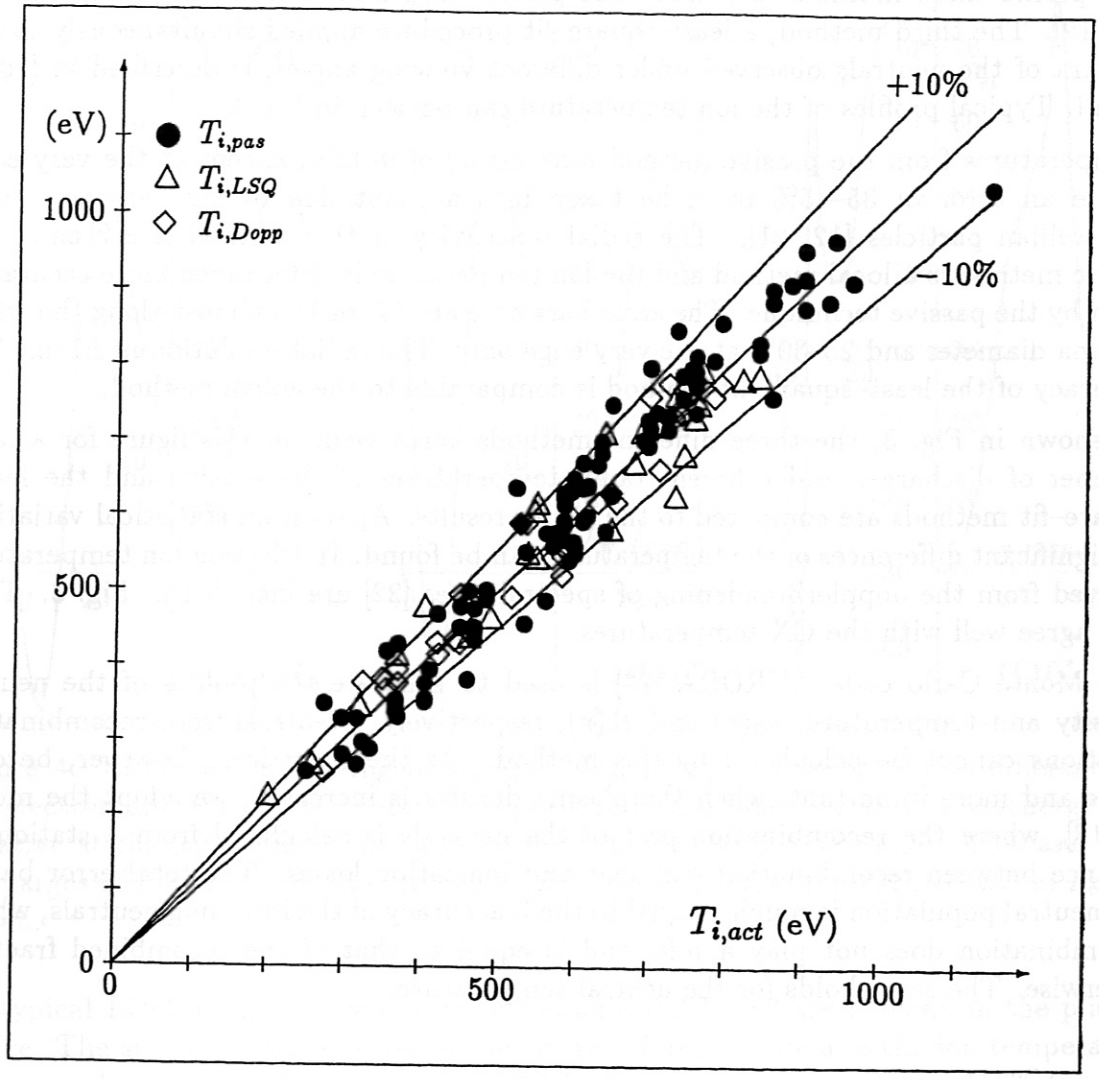

Figure 3: Comparison of ion temperatures at different radii obtained with different methods: passive CX (circles), least–square–fit (triangles) and spectroscopic measurements (diamonds) with results from active CX. Except for statistical variations, all methods yield almost identical values.

4.8×10^{19} m^{-3} (IOC), respectively.

The relative error of Z_{eff}, including both the variation during one stationary phase and the larger shot to shot variance, is 10–15% [17]. The higher value of 15% corresponds to low–density discharges. With the error bars discussed until now, the relative error of the ion density is calculated to $\Delta n_i(r)/n_i(r) = 6\% \times \sqrt{1 + 9 \times (n_e(r)/n_i(r) - 1)^2}$, with the first part within the square–root from the electron density and the second from the inaccuracies of Z_{eff} and Z_{imp}.

The ion temperature is measured using a neutral particle analyzer. A series of identical discharges is needed to measure the radial profile of the ion temperature. To determine

this profile three methods are used: the passive and active methods as explained in [18, 19]. The third method, a least–square–fit procedure applied simultaneously to flux spectra of the neutrals observed under different viewing angles, is described in [20] in detail. Typical profiles of the ion temperature can be seen in Fig. 2.

Temperatures from the passive method have errors of 9–13%, except at the very edge, where an error of 35–45% must be taken into account due to high–energetic non-maxwellian particles [12, 21]. The radial sensitivity of this method is ±2 cm. The active method is a local method and the ion temperature is determined more accurately than by the passive technique. The error bars here are 5% or less almost along the whole plasma diameter and 25–30% at the very edge only. The radial resolution is ±1cm. The accuracy of the least–square–fit method is comparable to the active method.

As shown in Fig. 3, the three different methods agree well. In this figure for a large number of discharges and different radii, temperatures of the passive and the least–square–fit methods are compared to the active results. Apart from statistical variations no significant differences of the temperatures can be found. In addition ion temperatures derived from the dopplerbroadening of spectral lines [22] are included in Fig. 3. They also agree well with the CX temperatures.

The Monte Carlo code AURORA [23] is used to generate the profiles of the neutral density and temperature, $n_0(r)$ and $T_0(r)$, respectively. Neutrals from recombination reactions cannot be calculated by this method. As these particles, however, become more and more important, when the plasma density is increased, we adopt the model of [18], where the recombination part of the neutrals is calculated from a stationary balance between recombination reactions and ionization losses. The total error bar of the neutral population is roughly equal to the inaccuracy of the incoming neutrals, where recombination does not play a role, and is equal to that of the recombined fraction otherwise. The same holds for the neutral temperature.

4 Sources and Losses

In this part we describe the source and loss terms of the local ion power balance, except for the ion heat conduction, which is described in chapter 6. We discuss the importance of these terms for the LOC, SOC and IOC regimes as a function of the plasma density. An error analysis is also presented.

4.1 The Electron–Ion Heating Power

In ohmic plasmas the only heating source for the ions is given by the electron–ion term Q_{ei}, which is proportional to the expression $n_e^2(T_e - T_i)/T_e^{3/2}$. All quantities in this definition are available from direct measurements.

Apart from the absolute values of Q_{ei}, its accuracy, too, is of interest for the solution of the power balance equation of the ions. The relative error of Q_{ei} in principle grows faster than the ratio T_i/T_e. Normally this ratio exceeds 0.9 under ohmic conditions, except

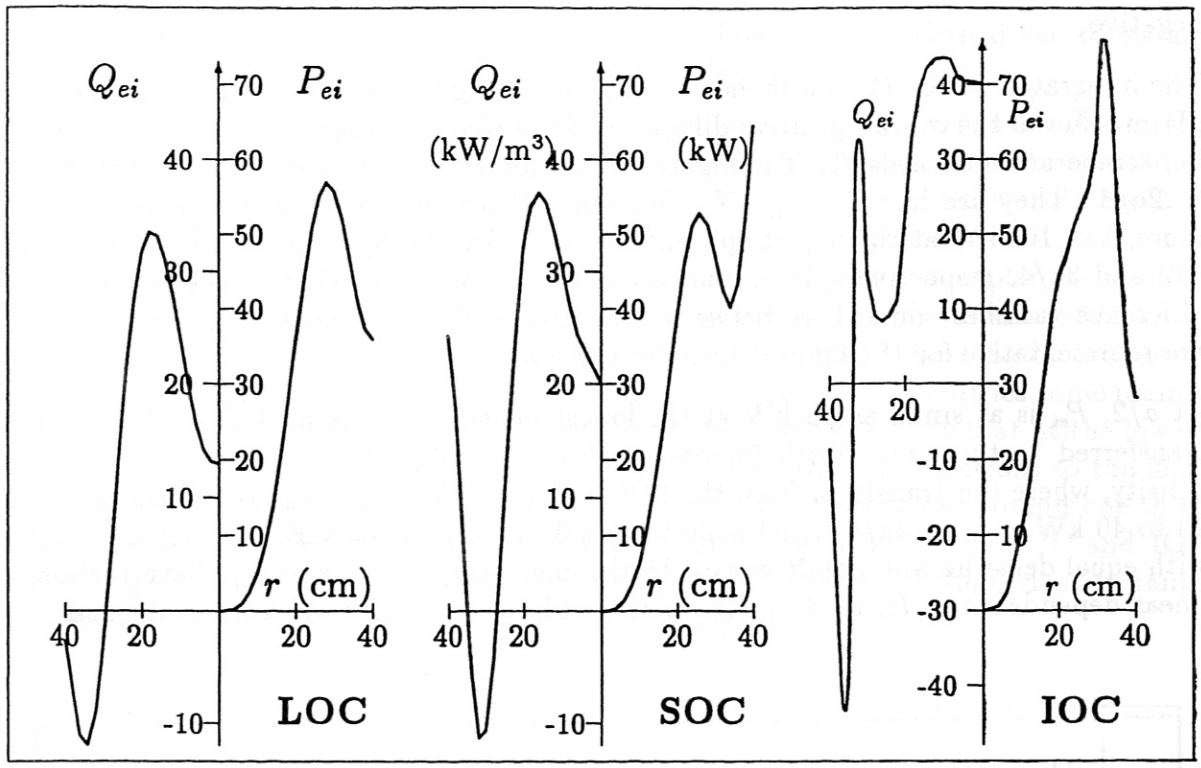

Figure 4: Electron–ion heating power Q_{ei}. Q_{ei} being a function of the difference of the electron and the ion temperature is positive in the inner region of a discharge and negative at the outer part. The profiles shown here belong to the LOC, SOC and IOC discharges of Fig. 2. In addition to the local power density, the integrated values P_{ei} are shown.

for typical LOC discharges, where values around 0.7 to 0.8 are reached in the plasma centre. The small difference between the electron temperature and the ion temperature causes a relative error of Q_{ei} of around 90% in the centre and more than 100% for radii larger than $a/2$. For LOC discharges a relative error of around 75% must be taken into account in the central region. But even for these discharges the error grows to values not less than 90% at radii larger than about $a/3$ to $a/2$.

The integrated power P_{ei} is used to overcome this problem at least for the innermost plasma region. The relative error of this term is dominated by the central error of the power density because of the smaller influence of the decreasing density and the decreasing temperature difference at higher radii. For LOC discharges P_{ei} is calculated with an accuracy better than about 80 to 90% at all radii. For SOC and IOC discharges, however, in general the absolute error exceeds the transferred power at almost all radii.

In Fig. 4 radial profiles of Q_{ei} and P_{ei} are shown for the discharges as in Fig. 2. In all cases the local power density Q_{ei} is positive in the inner part of the plasma, where the electron temperature surpasses the ion temperature. In the confinement region around $a/2$ to $3a/4$ the power density in general drops rapidly. Here $T_e - T_i$ almost vanishes. In the outer part of the discharges, where the ion temperature exceeds the electron temperature, an energy transfer from the ions to the electrons takes place and the Q_{ei}–term becomes

negative.

The integrated power P_{ei} is a monotonically increasing function in the inner part of the plasma due to the overall positive difference of the temperatures; it decreases where the ion temperature exceeds T_e. The highest values for P_{ei} are reached at radii around $a/2$ to $2a/3$. They are in the range of a few ten kW for the lowest densities and can be more than 100 kW at the highest plasma densities. In Fig. 5, P_{ei} is shown for two radii, $a/2$ and $3a/4$, respectively, as a function of $\overline{n_e}$. In ohmic discharges the temperature difference vanishes somewhere between these two radii. Therefore, these values of P_{ei} are representative for the highest transferred power.

At $a/2$, P_{ei} is as small as 10 kW at the lowest densities, while at $3a/4$ 20–30 kW are transferred to the ions. With increasing plasma density, P_{ei} increases, too. At the density, where the transition from the LOC to the SOC occurs, $P_{ei}(a/2)$ reaches about 20 to 40 kW and $P_{ei}(3a/4)$ reaches 30 to 70 kW. In Fig. 5 the variations for discharges with equal densities are mainly caused by the inaccuracy of Q_{ei} and P_{ei}. Nevertheless, a linear dependence of P_{ei} on $\overline{n_e}$ in the LOC can be seen clearly. This linear dependence

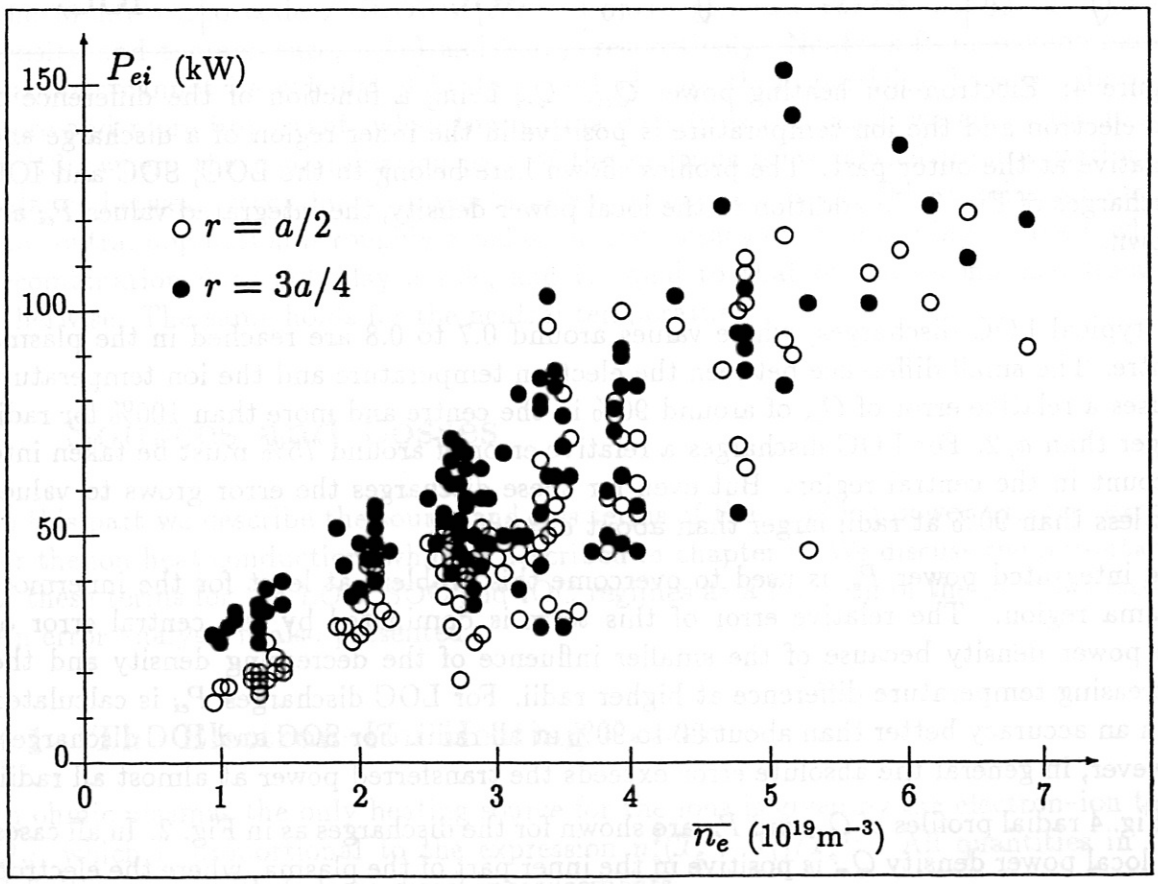

Figure 5: The integrated electron–ion–heating power depends linearly on the plasma density. Values for two different radii, $a/2$ (open circles) and $3a/4$ (full circles), start at 10–30 kW and end up at about 100 kW.

is consistent with the high–density regimes, too, although, the statistical variations are larger due to the large error of P_{ei} at high plasma densities.

A comparison of P_{ei} with the ohmic input power shows that the energy losses due to the ion energy transport play only a minor role to the total energy losses. For the discharges of our database the total ohmic power is 300–400 kW in all three confinement regimes. The power, which is lost via the ion energy transport, however, is restricted to P_{ei}. For LOC discharges, this is only one third of P_{OH} at the most. This is explained in more detail in Fig. 6. Organized in the same manner as Fig. 5, this figure shows the ratio of P_{ei} to the ohmic power P_{OH} for the two radii $a/2$ and $3a/4$. Here the ohmic power $P_{OH}(a/2)$ and $P_{OH}(3a/4)$, respectively, is used. Variations at fixed densities come mainly from variations of the ohmic power. Nevertheless, Fig. 6 shows clearly that at the lowest densities only one tenth of the ohmic input is transferred from the electrons to the ions. This ratio P_{ei}/P_{OH} increases with increasing density. It reaches values around one third for $a/2$ but is less than 20% for $3a/4$ at the transition density. In the SOC and IOC regime P_{ei}/P_{OH} increases only slightly at both radii. For the whole high–density range this ratio is 10–35% at $a/2$ and about 10–30% at $3a/4$.

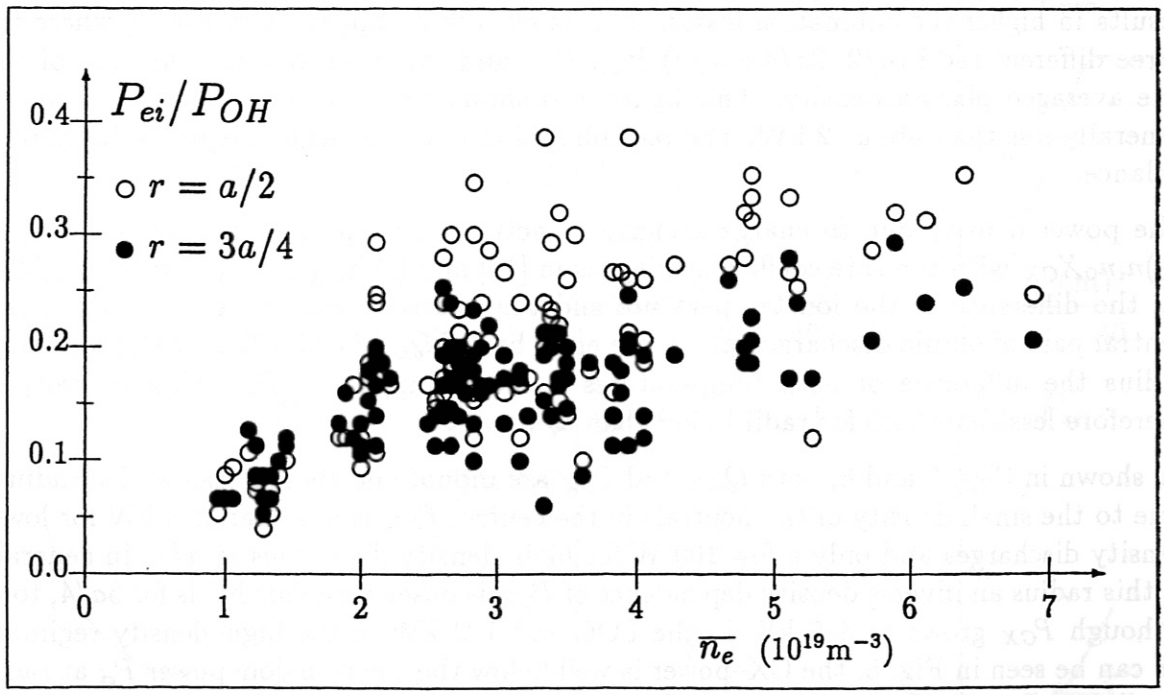

Figure 6: At low densities only 10 percent of the total ohmic power are transferred to the ions. Although there is a linear dependence of the ratio shown here on the plasma density even at the highest densities not more than about one third is lost via the ion branch.

In summary, in spite of the emphasis which has been put into the precise measurement of the ion temperature profile the small difference between the electron and the ion temperatures does not reduce the error in Q_{ei} and P_{ei} below about 90% in all three regimes. As P_{ei} is the dominant term of the integrated ion power balance equation,

solving this balance straight forward passes the same inaccuracy to its results. Our second conclusion is that at the most only one third of the ohmic power is transferred from the electrons to the ions. Therefore, the ion energy transport cannot dominate the total energy transport in any of the three ohmic confinement regimes. Hence, ohmic discharges are dominated by electron energy transport.

4.2 Neutral Particle Contributions

Recombination reactions, charge exchange reactions and ionization processes are three further terms in the power balance of the ions, i.e. losses Q_{rec} and Q_{CX} and a gain Q_{eii}, respectively.

Fig. 7 shows radial profiles of the power densities, Q_{rec}, Q_{CX} and Q_{eii} and their correlated integrated powers for three different discharges. Q_{rec} is almost constant in the inner part up to half of the plasma radius. In the outer part a fast decrease due to the descending ion and electron densities is observed. Comparing the profiles for the different discharges, with their averaged densities rising from LOC to IOC, shows that a higher plasma density results in higher recombination losses. This is even more apparent in Fig. 8, where for three different radii ($a/2$, $3a/4$ and a) P_{rec}, P_{CX} and P_{eii} are given as a function of the line averaged plasma density. This figure also shows that the recombination power is generally less than about 2 kW. The recombination power is negligible in the ion power balance.

The power density due to charge exchange reactions is proportional to $Q_{CX} \sim (T_i - T_0) n_i n_0 X_{CX}$ with the rate coefficient X_{CX} as in [10] and $(\Delta X_{CX})/X_{CX} \approx 0.5(\Delta T_i)/T_i)$. As the difference of the ion temperature and the neutral temperature is small in the central part of ohmic discharges, there the error bar of Q_{CX} is 50–70%. With increasing radius the difference of both temperatures is increasing, too. The relative error, is therefore less than 25% for radii larger than $a/4$.

As shown in Figs. 7 and 8, both Q_{CX} and P_{CX} are monotonically increasing with radius. Due to the small density of the neutrals in the centre, P_{CX} is less than 2–3 kW for low–density discharges and only a few 100 W for high–density discharges at $a/2$. In general, at this radius an inverse density dependence of P_{CX} is observed. This holds for $3a/4$, too, although P_{CX} grows to 4–7 kW in the LOC and 1–3 kW in the high–density regimes. As can be seen in Fig. 8, the CX–power is well below the electron–ion–power P_{ei} at radii smaller than r=$3a/4$. At the lowest densities P_{ei} is higher than P_{CX} by a factor of 10–20. Here the CX–losses are negligible. Only in the edge region a substantial amount of 10–15 kW is transferred to the neutrals, due to the steep increase of the neutral density. The situation at the edge is similar for all discharges, because the densities and temperatures there are similar and depend hardly on the central plasma density. At the plasma edge CX–losses must not be neglected.

A similar behaviour is observed for Q_{eii} and P_{eii}. Q_{eii} is described by $Q_{eii} = (3/2) T_0 n_0 n_e X_{eii}$ with X_{eii} from [11]. The error of Q_{ei} is dominated by the uncertainty of the neutral density. Hence, as an upper limit twice the error of n_0 can be assumed.

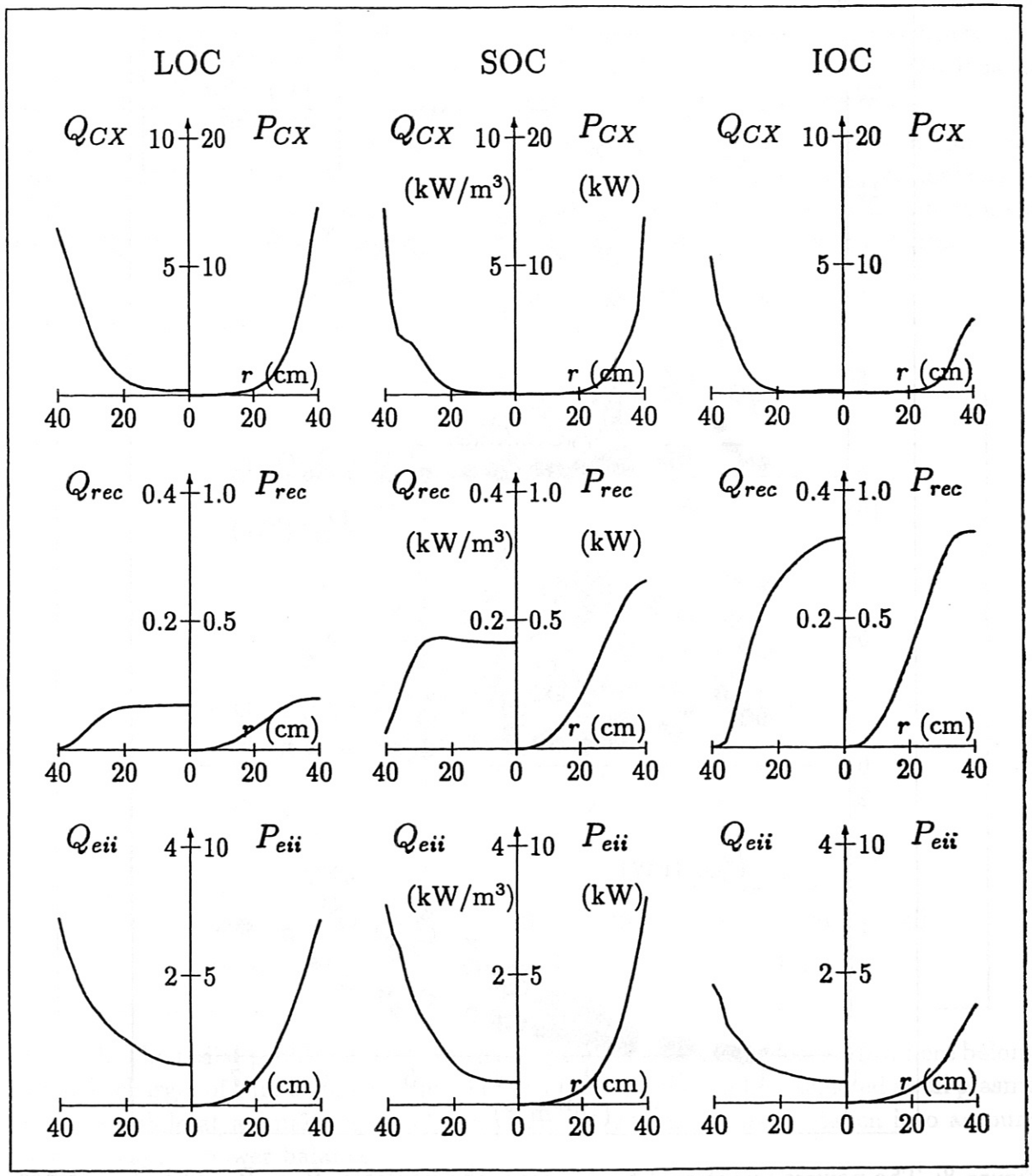

Figure 7: The power densities Q_{CX} (charge exchange), Q_{rec} (recombinations) and Q_{eii} (ionizations) and their integrated values for the discharges shown in Fig. 2 as functions of the plasma radius.

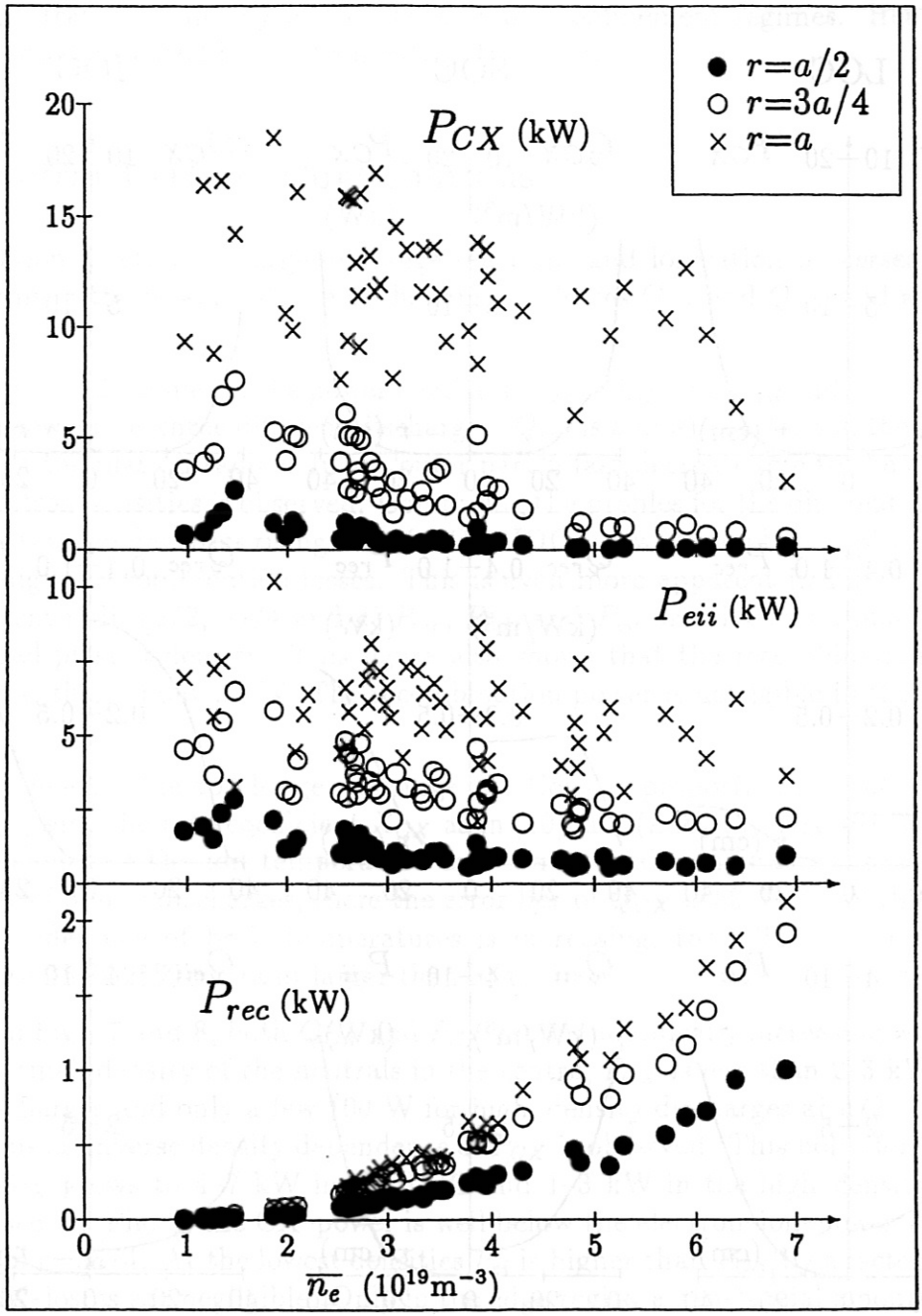

Figure 8: The powers transferred to and from the neutrals, P_{CX}, P_{eii} and P_{rec}, respectively, are given for three different radii ($a/2$, $3a/4$ and a) and for a large variety of discharges with different plasma densities. While P_{rec} can be neglected due to the small power transfer, both other mechanisms must only be taken into account at higher radii.

As illustrated in Figs. 7 and 8, Q_{eii} and P_{eii} are similar in magnitude to Q_{CX} and P_{CX}. The ionization gain is a more or less direct result of earlier losses in CX–reactions. Small differences between the ionization power and the CX–power in the plasma centre are mainly due to the different reaction cross–sections. At the edge, cold neutrals contribute only little to the ionization power. There the ionization gain is below the charge–exchange losses. The importance of P_{eii} on the power balance of the ions is comparable to that of P_{CX}. P_{eii} must be taken into account only at the edge.

Summarizing the influence of the three terms related to neutral particles, it must be remarked that only in a region around the plasma edge charge exchange and ionization effects are important. Elsewhere both channels influence the ion energy transport only marginally. The recombination reactions can be neglected for the power balance.

4.3 Convective Losses

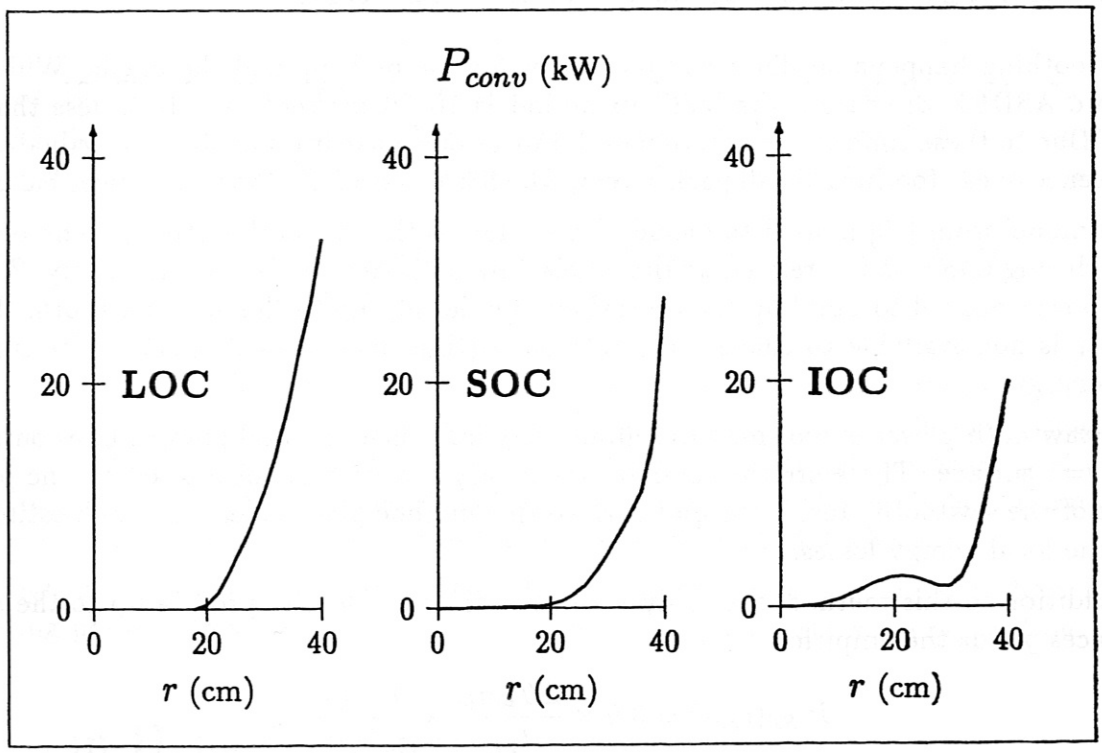

Figure 9: The radial profiles of the (integrated) convective energy loss shown here belong to the discharges of Fig. 2. In the central region these losses can be neglected at all plasma densities, while at a small region at the plasma edge they must be taken into account for the local ion power balance.

In a steady–state plasma convective particle losses, recombinations and ionization are in balance. Integrating the particle balance equation and using Eq. (4) gives the convective energy flux. In Fig. 9 radial profiles are shown for the three confinement regimes.

In the central region recombination and ionization tend to balance each other. Hence, convective losses are negligible here.

In the outer part of the plasma recombinations can be neglected. Here convection balances the ionization processes. Hence, the error is comparable to the error of the ionization power P_{eii}. Since the ionization rate increases with neutral density the convective fluxes show a strong increase towards the plasma edge. Fig. 9 illustrates an inverse plasma density dependence of the convective fluxes in the outer part of the discharges. For low–density discharges up to 30–40 kW are reached at the edge. In discharges with high plasma densities only 20–30 kW are transported via convective fluxes.

It can be summarized that for low–density plasmas convective losses must not be neglected in the outer 15 cm of the plasma. Due to the density dependence, the importance of this mechanism is decreasing with growing plasma density. For high–density discharges convective energy losses enter the ion power balance only in a small region at the plasma edge.

4.4 Energy Losses due to Sawtooth Activity

Sawtoothing happens on different time–scales for the built up and the crash. While in ohmic ASDEX discharges the built up period is 10–30 ms the crash lasts less than 1 ms. Due to these time scales experimental limitations make it impossible to evaluate the influence of sawtoothing on all parameters, which are needed for the local power balance.

The model from [20] is used to include losses due to the sawtooth–activity. The power lost during one crash is related to the whole sawtooth–period. In the same way P_{ST} is the power needed to build up the central energy density up to the next sawtooth. This power is not available to change the stationary (time–independent) part of the stored ion energy.

The sawtooth power is too small to significantly influence the total power fluxes outside the q=1 surface. Therefore the common stationary situation is not altered by the presence of the sawtooth. Inside the q=1 surface this method gives at least a rough estimate for the local energy losses.

In addition to this method, the analysis of several power density profiles up to the q=1 surfaces yields the empirical relation

$$P_{i,ST}(r_{q=1}) = 3.9 \times \frac{\Delta T_{i0} n_{i0}}{t_{ST}} \times \frac{1 - q_0}{q_a - q_0} \quad . \tag{5}$$

In Eq. (5) ΔT_{i0} denotes the central temperature difference before and after the crash (in eV) as determined with the model from [20] and n_{i0} is the central ion density (in 10^{19} m^{-3}). The sawtooth period t_{ST} (in seconds) and the central and edge value of the q–profile are needed, too. In low–q discharges this formula leads to a small overestimate, while for discharges with a central q_0 around unity a weak underestimation may occur. In moderate discharges, however, this equation can be used for fast analyses of sawtooth energy losses.

As indicated by Eq. (5) the sawtooth power depends strongly on the q profile. In high–q discharges sawtoothing appears only in the very centre. There P_{ST} is less than 1 kW at the q=1 surface. It increases to 20–30 kW for low–q discharges.

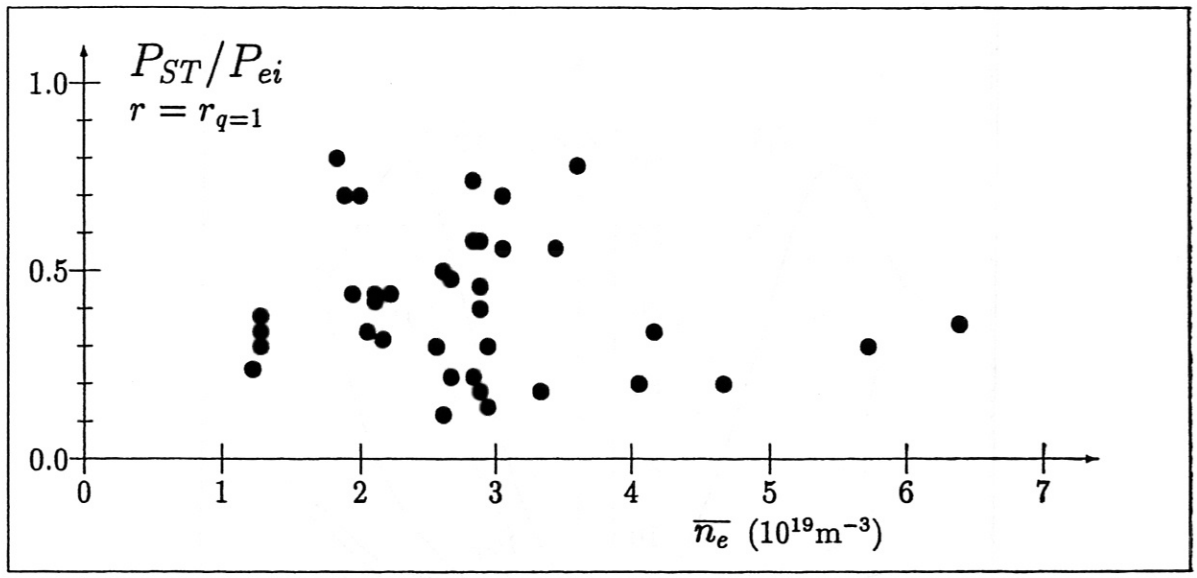

Figure 10: The fraction of the heating power lost by sawtooth activity inside the q=1–surface is shown here. This part is missing for the heating of the time–averaged and stationary part of a discharge if a quasi-stationary time–averaged power balance is used.

A comparison of P_{ST} from [20] with P_{ei} is given in Fig. 10. The ratio P_{ST}/P_{ei} is plotted as a function of the density at the q=1 surface

For LOC discharges a wide variation occurs in Fig. 10. This is mainly due to differing q profiles and ion densities. In LOC discharges sawtoothing accounts for up to 80% of P_{ei}. This strongly affects the ion power balance. A simple conclusion is that this enormous fraction cannot contribute to the heating of the normal stationary part of the discharge. At the worst only one fifth of the heating power is left over to heat the normal time–averaged fraction of the ions in the central part of LOC discharges.

In high–density discharges (SOC, IOC) the sawtooth power is about one third of the heating power. Only (2/3) $\times$ P_{ei} remains to heat the steady–state ion population.

5 Ion Heat Conduction

In this section we present the results concerning the losses due to the ion heat conduction and especially for the ion heat conductivity itself.

In Fig. 11 the ion power balance is shown for the selected LOC discharge (see Fig. 2). The sum of the integrated powers is given at the left hand side for all gains and at the right hand side for all losses. It can be seen that P_{ei} is the dominating heating term in the ion power balance of LOC discharges. The energy gain from the ionization of neutrals is by at least a factor of twenty smaller.

The situation at the right hand side of Fig. 11, i.e. the part handling all losses, is quite different. Although it gives the impression that heat conduction P_{hc} is responsible for

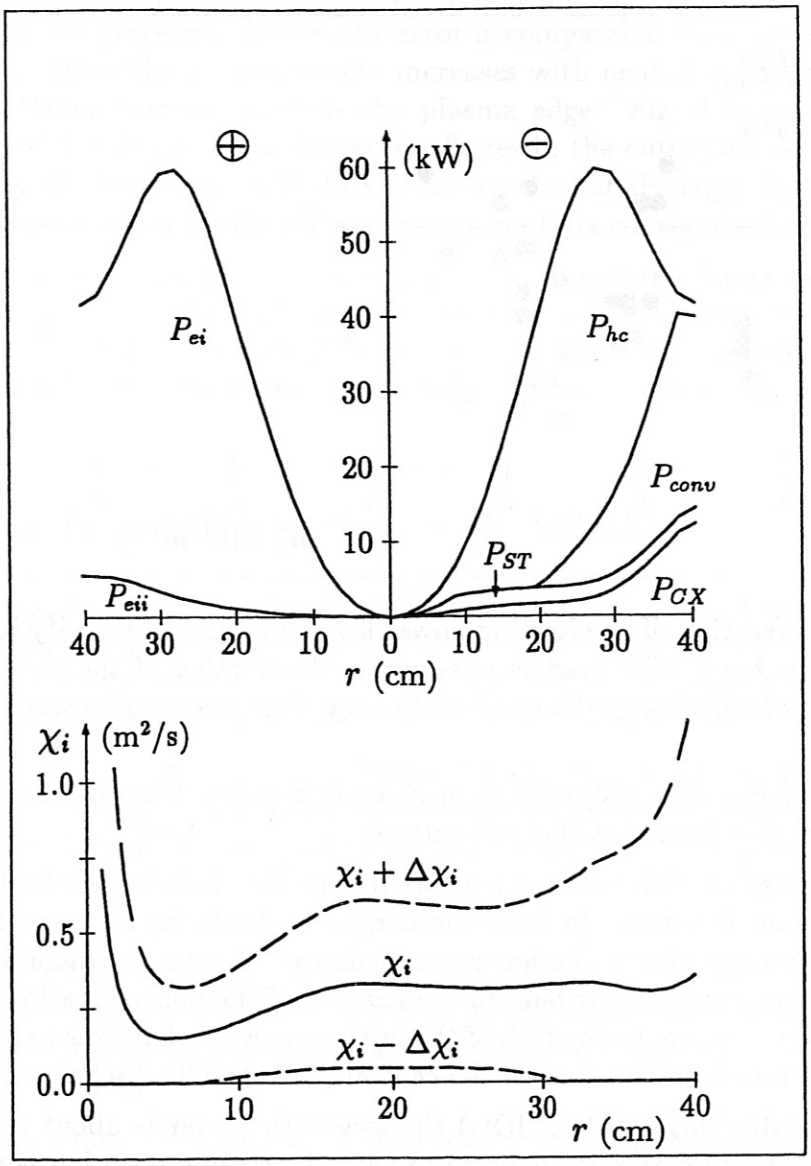

Figure 11: The power balance of the ions of the LOC discharge from Fig. 2 shows that the main mechanisms transporting energy to the plasma edge are heat conduction, sawtooth transport (centre only), convection (outside $a/2$) and charge exchange (edge only). Other mechanisms only play a minor role. The profile of the ion heat conductivity χ_i is typical for low-density discharges.

almost the whole energy transfer, three regions have to be distinguished. In the central region sawtooth-activity leads to a remarkable energy loss. In this example, with the q=1-surface close to $a/4$, about one third of the power input is lost by P_{ST}. Going to the confinement region around $a/2$ heat conduction dominates the energy losses. It balances almost the whole power input P_{ei}. At the plasma edge further mechanisms have to be taken into account. Convective fluxes increase strongly with increasing radius due to the steep profile of the neutral density. At the very edge this process may dominate the

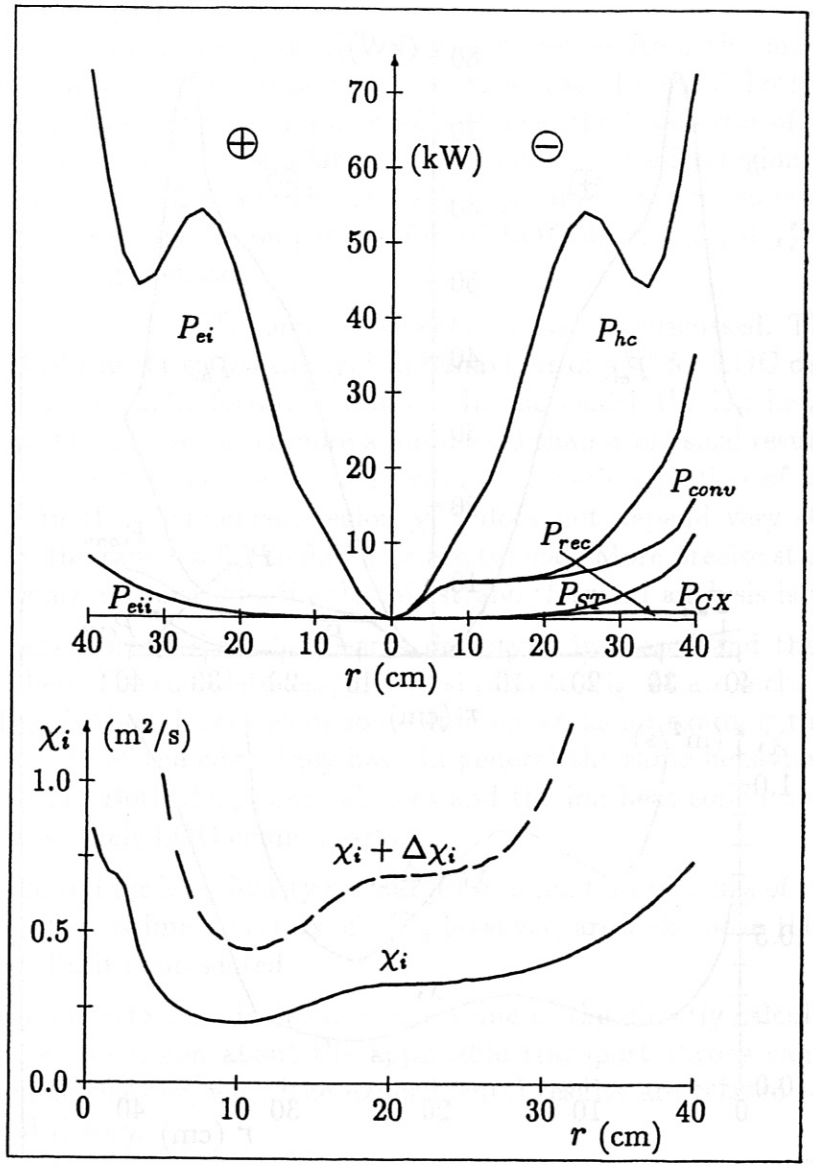

Figure 12: The power balance of the ions and the ion heat conductivity for the SOC discharge from Fig. 2 in principle shows the same behaviour as the LOC discharge of Fig. 11.

power balance. The other important loss mechanism is caused by CX–reactions, which also increase with the neutral density.

The experimental ion heat conductivity χ_i^{exp} obtained for this power balance is shown in the lower part of Fig. 11. The error of χ_i^{exp}, which is due to the errors discussed above, is marked by dashed lines. It is considered as a lower limit of the real error. A small error of the ion temperature profile around the centre causes errors for the ion temperature gradient which are larger than 100%. The confinement region shows a more favourable behaviour. In normal situations, the relative statistical error of the ion

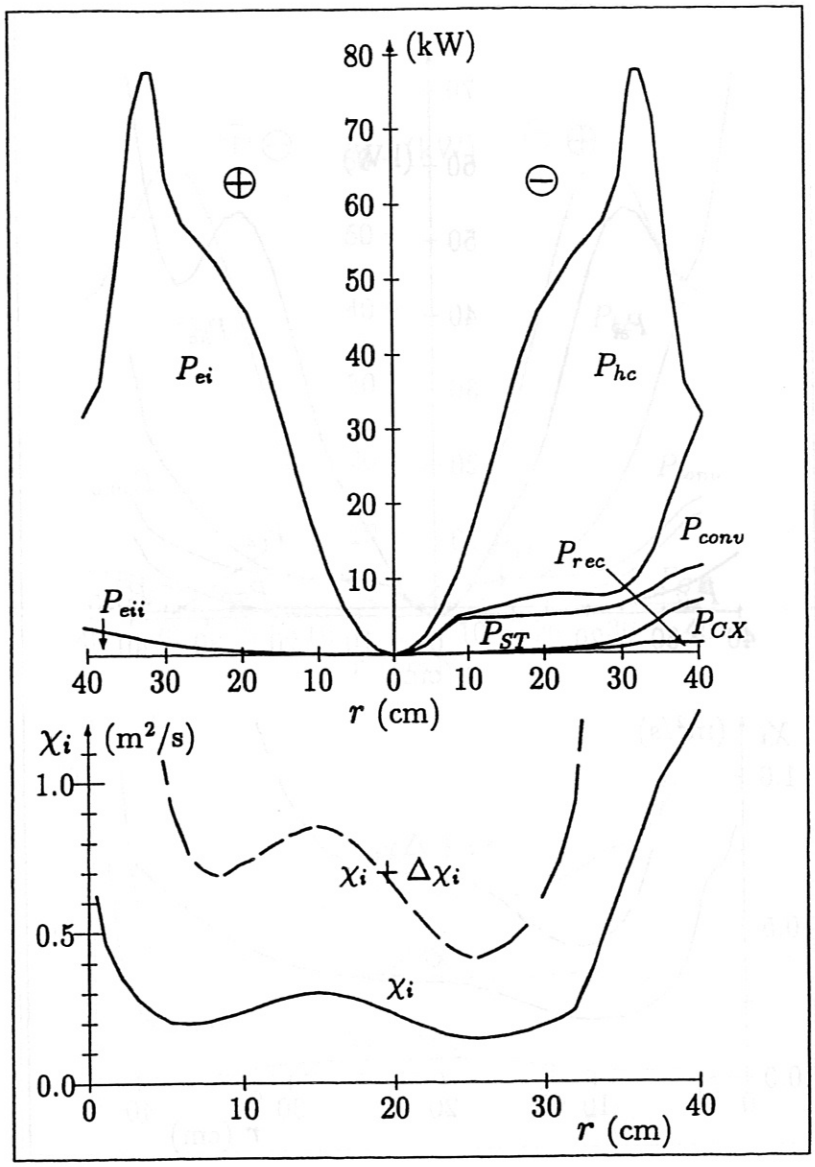

Figure 13: Power balance of the ions and χ_i^{exp} for the IOC discharge from Fig. 2, in principle similar to both other balances and conductivities.

temperature lies well below 10%. Two different mechanisms, however, may introduce errors here. The first one is the choice of a disadvantageous fitting function to get the gradient of the temperature profile. It, however, is minimized by cross-checking the results for different types of functions during our analyses, i.e. exponentials, polynomials and general polynomials with free exponents. The other one is a direct consequence of the steep shape of the temperature profile in this region. Because of the finite radial resolution of the CX-methods of 1 to 2 cm, the link of the radial position and an experimental T_i value normally results in a not controllable random error of the gradient. Comparisons of calculations, where the ion temperature and their associated radii are altered within their margins, show that the error due to the ambiguous gradient is 20–40

percent.
Despite the low quality of χ
The most important uncertainty of χ_i^{exp}, however, comes from the inaccuracy of the electron–ion–heating term. As discussed before, it is around 90%. All other terms in the power balance equation play only a minor role. Hence, the total error of χ_i^{exp} is close to 90% in this region. A situation similar to this exists for the edge region. The errors of heating power, convective flux and charge–exchange power sum up to more than 100%. This large error in the edge is comparable for all LOC discharges, if χ_i^{exp} is calculated by this straightforward method.

$_i^{exp}$, common aspects can yet be discussed. The curve given in the lower part of Fig. 11 shows the typical behaviour of χ_i^{exp} for LOC discharges when calculated with the straight–forward method. In the centre the ion heat conductivity tends to infinity. This, however, is more a numerical than a physical result owing to the vanishing ion temperature gradient which enters the basic equation of this method as a denominator. In the confinement region χ_i^{exp} does not depend very strongly on the radius. Values in the range of 0.1 to 0.6 m^2/s are typical. More precise statements about numerical values are not possible, if only this straightforward analysis is used.

The situation gets worse, when the plasma density is increased and the SOC or IOC regimes are reached. For completeness, figures similar to Fig. 11 are included (SOC: Fig. 12; IOC: Fig. 13). Although they show some differences, as for example the behaviour of the convective fluxes at the edge, they have in general the same behaviour as the LOC discharge in Fig. 11. Both the power balances and the ion heat conductivities show the same tendencies as their LOC counterparts.

The statements found for low–density discharges also hold for plasmas of these two high–density regimes. The estimated errors of χ_i^{exp}, however, are well above 100% at all radii, so only an upper limit is presented.

Despite the large uncertainties in the absolute value of the directly calculated heat conductivity, definite conclusion about the applicable transport theory can be drawn, as szhown in the next chapter, when the experimental results are related to expectations from neoclassical theory.

6 Comparison with Neoclassical Theory

In this section we compare the experimentally found ion heat conduction with neoclassical theory on the basis of [8]. Two methods are used: a direct comparison of χ_i^{exp} with χ_i^{neo} and a comparison of the measured ion temperature profiles with those predicted by the neoclassical theory.

Fig. 14 shows the radial profiles of the neoclassical ion heat conductivity and the experimental data of the discharges of Figs. 11–13. χ_i^{neo} agrees well with χ_i^{exp} in all three discharges. This result holds for the whole database. The experimental enhancement factor $\chi_i^{exp}/\chi_i^{neo}$ is shown in Fig. 15 for three radii as a function of the density. In this figure full circles denote LOC and SOC discharges, while IOC discharges are marked by open circles. Due to the large errors of χ_i^{exp} a large variation of these data occurs for

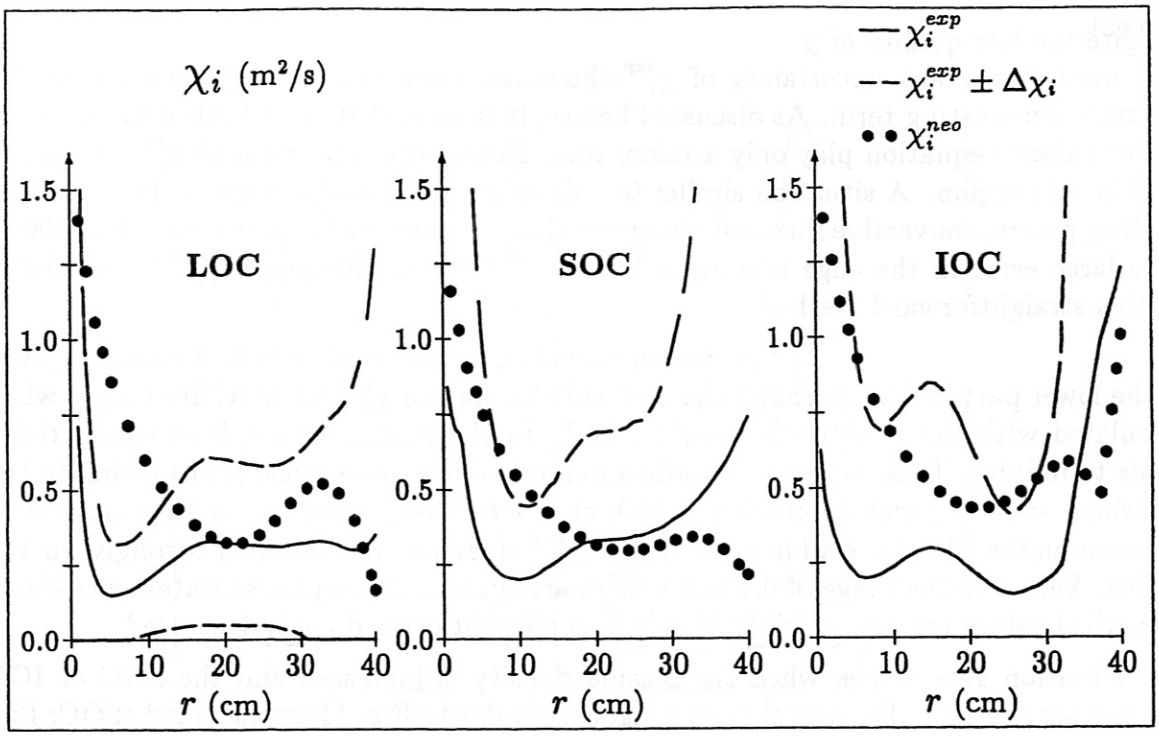

Figure 14: For all three discharges the neoclassical heat conductivity (dotted curve) lies close to χ_i^{exp}.

discharges at the same density. Nevertheless, averaged values are close to 1 in the LOC and SOC regimes and systematically lower than 1 in the IOC regime.

For LOC discharges the mean value of $\chi_i^{exp}/\chi_i^{neo}$ is 1.1±0.6 at radius $a/4$. An ion energy conductivity, which is significantly higher than neoclassical, can therefore be excluded. For the radius $a/2$ an average of 1.5±0.6 is determined. Here the neoclassical prediction is valid within the error bar, too. But also an ion heat conductivity of about two times neoclassical is possible. At the plasma edge, the mean ratio is again close to 1. The data points shown in Fig. 15 at $3a/4$, for example, give 0.9±0.6 for the LOC discharges. Similar to the inner region, a significant anomalous ion heat transport can be excluded.

The results for the SOC discharges are nearly identical to those of the LOC regime. The averages are 1.3±0.5 at $a/4$, 1.5±0.6 at $a/2$ and 0.6±0.5 at $3a/4$. Therefore, it is concluded that the ion heat transport mechanism is the same for LOC and SOC discharges. A somewhat different behaviour is obtained for IOC discharges. Here the mean values (0.3±0.2, 0.6±0.2, 0.7±0.3) are below one.

To confirm these results, a more accurate analysis method is used. With the assumption that the ion heat conductivity is neoclassical, ion temperature profiles are modelled for all discharges of our database. The error bars for the simulated temperatures are lower than 15%. To demonstrate the sensitivity of this method, ion temperature profiles are also simulated for two times and three times the neoclassical conductivity. These profiles are shown in Fig. 16, together with the experimental profiles. The neoclassical temperature profiles of all three discharges are close to the experimental profiles. Both profiles of the

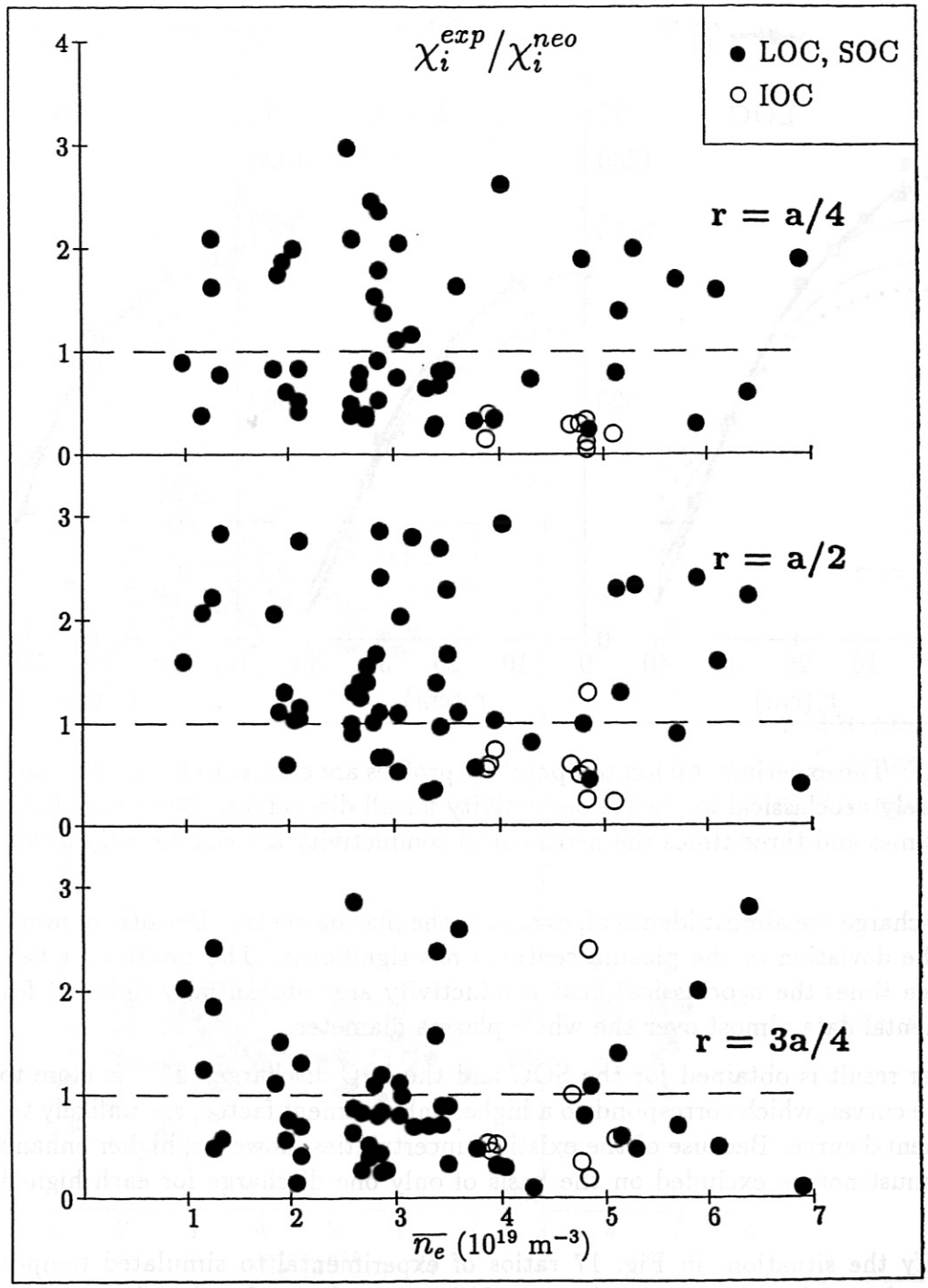

Figure 15: Here, the ratios of the experimental to the neoclassical χ_i belong to regions where sawtooth losses (a/4), pure conductive losses (a/2) and also convective losses (3a/4) influence the ion power balance.

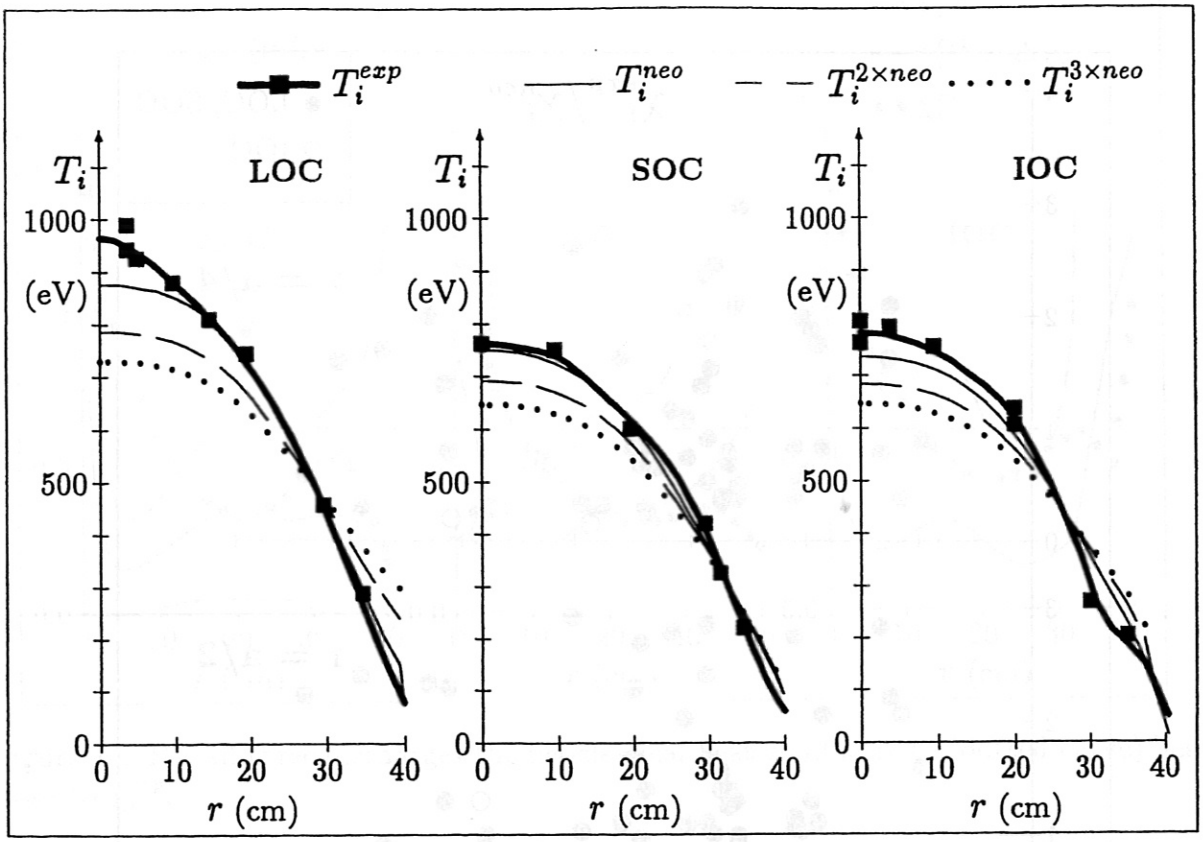

Figure 16: The experimental ion temperature profiles are closest to the profiles simulated with purely neoclassical ion heat conductivity for all discharges. The simulated profiles to two times and three times the neoclassical conductivity are significantly lower.

LOC discharge are almost identical, except in the plasma centre. Because of overlapping errors the deviation in the plasma centre is not significant. The profiles for two times and three times the neoclassical heat conductivity are substantially different from the experimental data almost over the whole plasma diameter.

A similar result is obtained for the SOC and the IOC discharge. T_i^{exp} is close to T_i^{neo}, while the curves, which correspond to a higher enhancement factor, are unlikely to fit the experimental curve. Because of the existing uncertainties, however, higher enhancement factors must not be excluded on the basis of only one discharge for each high-density regime.

To clarify the situation, in Fig. 17 ratios of experimental to simulated temperatures are plotted as a function of the density. Values are shown for the plasma centre and for $a/2$. The ratio increases with increasing enhancement factor for the conductivity, because of the decreasing simulated temperatures. For LOC discharges a definite result is obtained. All ratios corresponding to $1\times\chi_i^{neo}$ lie in a small region around unity. The neoclassical theory explains very well the experimental ion temperatures in the central part of all LOC plasmas. Ratios to $2\times\chi_i^{neo}$ and $3\times\chi_i^{neo}$ depart clearly from unity. Temperatures simulated with these enhanced conductivities are systematically too low,

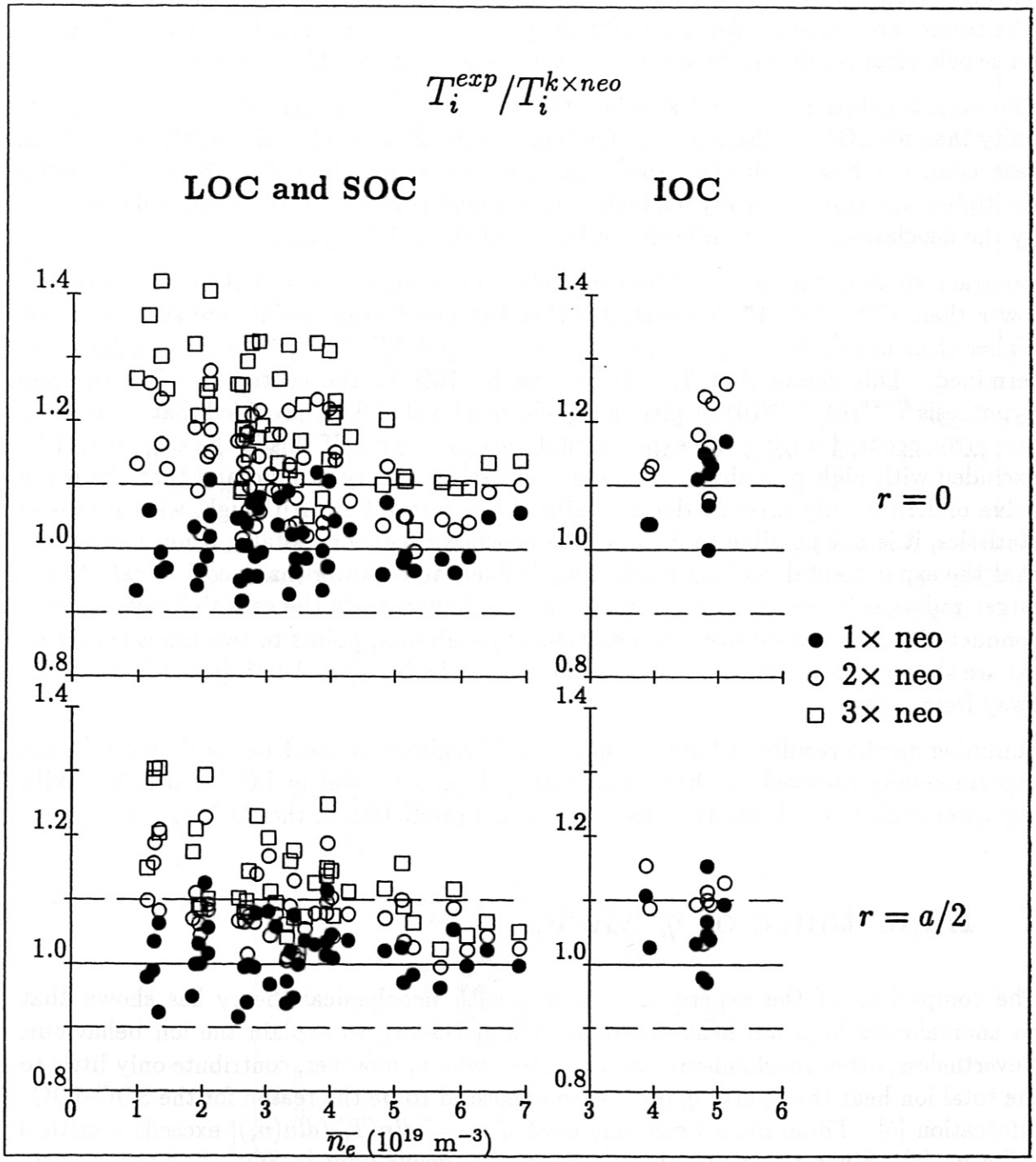

Figure 17: The ratios of experimental to neoclassical temperature in the centre and at $a/2$ for the different regimes.

even if the differences to the experimental values decrease with increasing density. The good agreement of T_i^{exp} and T_i^{neo} does not change across the whole plasma diameter. This is illustrated in the lower part of Fig. 17, where ratios for the radius $a/2$ are shown. The results are the same for $a/2$ as for the plasma centre, i.e. points very close to unity for neoclassical conductivity and values well above unity for higher conductivities.

The same conclusion can be drawn for SOC discharges. Although all ratios are closer to unity than for LOC discharges, even for higher multipliers to χ_i^{neo}, the purely neoclassical case coincides best with the experiment over the whole diameter. Ratios to higher multipliers are systematically too high. The ion heat transport is therefore well explained by the neoclassical theory in both the LOC and the SOC regime.

Contrary to this, the neoclassically predicted ion temperatures of IOC discharges are lower than T_i^{exp}. Fig. 17 demonstrates that the neoclassical points are systematically higher than unity. In the plasma centre an averaged $T_i^{exp}(0)/T_i^{neo}(0)$=1.13±0.06 is determined. This shows that T_i^{neo} is too low by 10% in the centre. Testing the null hypothesis $T_i^{exp}(0)/T_i^{neo}(0)$=1 gives a significance level of 0.07, provided that no systematic error occured during the experimental measurements. If this is the case, it can be excluded with high probability that the neoclassical theory is valid and that the mean value of 1.13 is only a result due to statistical uncertainties. Although, with means of statistics, it is not possible to disprove the neoclassical theory totally, it must be stated that the experimental ion heat conducivity is likely to be lower than neoclassical. At the larger radius $a/2$ the average is 1.06±0.06. To demonstrate the sensitivity, if the heat conductivity is increased over the neoclassical prediction, points to two times neoclassical are shown in Fig. 17, too. Their averages are 1.18 (r=0) and 1.15 (r=$a/2$), being far away from unity.

Summing up the results of both methods for all regimes, it must be concluded that the experimentally resolved ion heat conductivity is neoclassical in LOC and SOC. With high probability, it is lower than the neoclassical prediction in the IOC regime.

7 Importance of η_i Modes

The comparison of the experimental results with neoclassical theory has shown that no anomalously high ion heat conductivity is necessary to explain the ion behaviour. Nevertheless, other mechanisms can occur, too, which, however, contribute only little to the total ion heat transport. η_i modes are suggested to be the reason for the SOC–IOC–bifurcation [5]. These modes can only exist if $\eta_i = |dln(T_i)/dln(n_i)|$ exceeds a critical value η_{ic} [4]. Since these modes are expected to occur only in SOC discharges, there $\eta_i > \eta_{ic}$ must be fulfilled.

To determine whether or not these modes can occur in ohmic discharges at all, radial profiles of both the experimental η_i and the critical η_{ic} are shown in Fig. 18. For all three discharges a region is found, where η_i exceeds the critical value. There is no significant difference between the three discharges and the different confinement regimes. This is even more apparent in Fig. 19. There the largest ratio of η_i^{exp} to η_{ic} along the whole

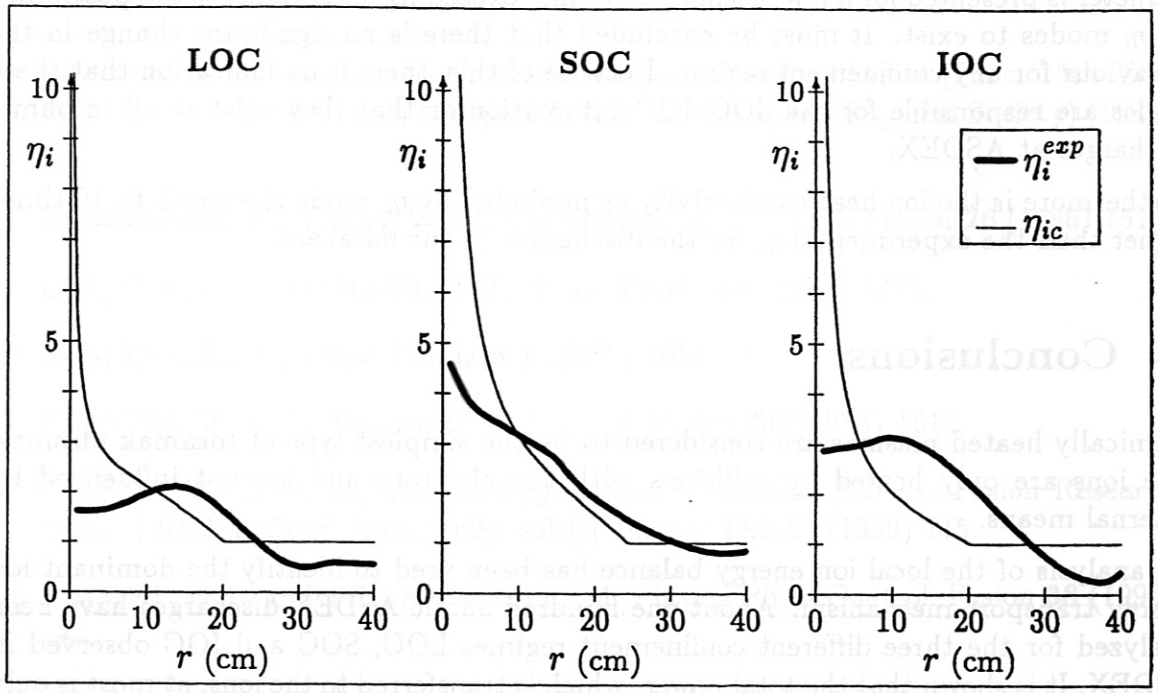

Figure 18: Additional heat conductive losses due to η_i modes are expected only for regions with $\eta_i(r)$ exceeding the critical $\eta_{ic}(r)$. In general, this condition is fulfilled in the confinement region of an ohmic plasma. The curves shown here belong to the discharges of Fig. 2.

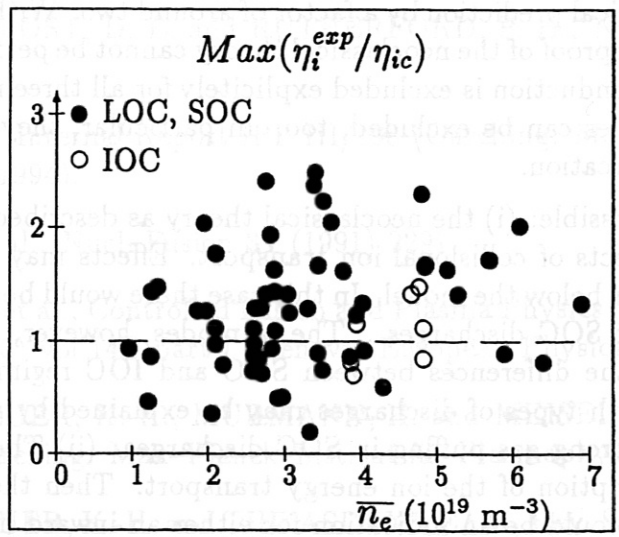

Figure 19: The maximum value of η_i^{exp}/η_{ic} along the whole plasma radius shows whether η_i modes are expected to occur (> 1) or not (< 1). The data of all three ohmic confinement regimes show no significant differences between LOC and SOC or SOC and IOC discharges.

diameter is presented for a few discharges. Points exceeding unity indicate the possibility for η_i modes to exist. It must be concluded that there is no significant change in the behaviour for any confinement regime. Because of this, there is no indication that these modes are responsible for the SOC–IOC–bifurcation or that they exist at all in ohmic discharges at ASDEX.

Furthermore is the ion heat conductivity as predicted by η_i–mode theories 5 to 10 times higher than the experimental χ_i for the discharges in our database.

8 Conclusions

Ohmically heated plasmas are considered to be the simplest type of tokamak plasmas. The ions are only heated by collisions with the electrons and are not influenced by external means.

An analysis of the local ion energy balance has been used to identify the dominant ion energy transport mechanism. About one hundred ohmic ASDEX discharges have been analyzed for the three different confinement regimes LOC, SOC and IOC observed in ASDEX. It is shown that the total power, which is transferred to the ions, at most is only one third of the ohmic power. Hence, the local energy transport of the whole plasma is dominated by the electron energy transport in all confinement regimes.

The analysis of the ion heat conductivity shows that in both, the LOC and the SOC regime, the experimental ion temperature and ion heat conductivity are well explained by neoclassical theory. For the IOC regime the measured conductivity is found to be lower than the neoclassical prediction by a factor of around two. With means of statistics, however, a complete disproof of the neoclassical theory cannot be performed. Higher than neoclassical ion heat conduction is excluded explicitely for all three regimes. Anomalous mechanism like η_i modes can be excluded, too. In particular, they are not responsible for the SOC–IOC bifurcation.

Two conclusions are possible: (i) the neoclassical theory as described in [8] does not give full account of all aspects of collisional ion transport. Effects may be neglected, which produce transport rates below the model. In this case there would be room for anomalous ion transport in ohmic SOC discharges . The η_i modes, however, would still not be a candidate to explain the differences between SOC and IOC regime. In this case the differences between both types of discharges may be explained by additional turbulent processes due to the strong gas puffing in SOC discharges. (ii) The neoclassical model [8] is a complete description of the ion energy transport. Then the high experimental T_i in the IOC regime would be an indication for either an inward heat pinch in the ion channel or for anomalously high energy transfer rates from the electrons to the ions.

References

[1] MÜLLER, E. R. et al., Controlled Fusion and Plasma Physics (Proc. 15th Eur. Conf. Dubrovnik, 1988) vol 12B part I (Geneva: European Physical Society) (1988) 19.

[2] ROMANELLI, F., TANG, W. M. and WHITE, R. B., Nucl. Fusion **26** (1986) 1515.

[3] LEE, G. S. and DIAMOND, P. H., Phys. Fluids **29** (1986) 3291.

[4] ROMANELLI, F., Phys. Fluids B **1** (1989) 1018.

[5] GRUBER, O. et al., Plasma Phys. Control. Fusion **30** (1988) 1611.

[6] FUSSMANN, G. et al., Plasma Physics and Controlled Nuclear Fusion Research (Proc. 12th Int. Conf. Nice, 1988) vol 1 (Vienna: IAEA) (1989) 145.

[7] SIMMET, E. E. and THE ASDEX TEAM, Plasma Phys. Control. Fusion **38** (1996) 689.

[8] CHANG, C. S. and HINTON, F. L., Phys. Fluids **29** (1986) 3314.

[9] GORDEEV, Y. S., ZINOV'EV, A. N. and PETROV, M. P., Sov.Phys.–JETP Lett. **25** (1977) 204.

[10] RIVIERE, A. C., Nucl. Fusion **11** (1971) 363.

[11] DÜCHS, D. F., POST, D. E. and RUTHERFORD, P. H., Nucl. Fusion **17** (1977) 565.

[12] SIMMET, E. E., Internal Report IPP III/198 (Garching: Max–Planck–Institut für Plasmaphysik) (1994).

[13] STROTH, U. et al., Nucl. Fusion **31** (1991) 2291.

[14] STEUER, K.-H. et al., Controlled Fusion and Plasma Physics (Proc. 17th Eur. Conf. Amsterdam, 1990) vol 14B part I (Geneva: European Physical Society) (1990) 62.

[15] RÖHR, H., STEUER, K.-H., MURMANN, H. and MEISEL, D., Internal Report IPP III/121 (Garching: Max–Planck–Institut für Plasmaphysik) (1987).

[16] RÖHR, H., STEUER, K.-H. and THE ASDEX TEAM, Rev. Sci. Instrum. **59** (1988) 1875.

[17] STEUER, K.-H., RÖHR, H. and KURZAN, B., Rev. Sci. Instrum. **61** (1990) 3084.

[18] AFROSIMOV, V. V. and KISLYAKOV, A. I., Diagnostics for Fusion Reactor Conditions (Proc. Int. Conf. Varenna, 1982) vol 1 (Brussels: Commission of the European Communities) (1982) 289.

[19] FAHRBACH, H. U., HERMANN, W. and MAYER, H. M., Controlled Fusion and Plasma Physics (Proc. 16th Eur. Conf. Venice, 1989) vol 13B part IV (Geneva: European Physical Society) (1989) 1537.

[20] STROTH, U., FAHRBACH, H.-U., HERRMANN, W. and MAYER, H.-M., Nucl. Fusion **29** (1989) 761.

[21] SCHNEIDER, R., VERBEEK, H., REITER, D., NEUHAUSER, J. and THE ASDEX TEAM, Controlled Fusion and Plasma Physics (Proc. 18th Eur. Conf. Berlin, 1991) vol 15C part III (Geneva: European Physical Society) (1992) 117.

[22] CHU, C. C., NOLTE, R., FUSSMANN, G., FAHRBACH, H. U., HERRMANN, W., SIMMET, E. and ASDEX-TEAMS, Controlled Fusion and Plasma Physics (Proc. 18th Eur. Conf. Berlin, 1991) vol 15C part IV (Geneva: European Physical Society) (1992) 297.

[23] HUGHES, M. H. and POST, D. E., J. Comp. Phys. **28** (1978) 43.